ACS APPLIED MATERIALS & INTERFACES

www.acsami.org Research Article

Aptamer-Functionalized Three-Dimensional Carbon Nanowebs for Ultrasensitive and Free-Standing PDGF Biosensor

Wooyoung Kim, Jun Seop Lee,* and Jyongsik Jang*

Cite This: *ACS Appl. Mater. Interfaces* 2020, 12, 20882−20890 Read Online

ACCESS | Metrics & More | Article Recommendations | Supporting Information

ABSTRACT: Research on flexible biosensors is mostly focused on their use in obtaining information on physical signals (such as temperature, heart rate, pH, and intraocular pressure). Consequently, there are hardly any studies on using flexible electronics for detecting biomolecules and biomarkers that cause diseases. In this study, we propose a flexible, three-dimensional carbon nanoweb (3DCNW)-based aptamer sensor to detect the platelet-induced growth factor (PDGF), which is an oncogenic biomarker. As a template for the 3D structure, poly(acrylonitrile) (PAN) nanowebs were synthesized using a facile electrospinning process. The PAN nanowebs were then subjected to chemical vapor deposition with copper powder. This was followed by Cu etching to generate carbon protrusions on the web surface. As an active site, PDGF-B binding aptamer was introduced on the 3DCNW surface to form biosensor electrodes. The 3DCNW-based aptasensor exhibited excellent sensitivity (down to 1.78 fM), with high selectivity, reversibility, and stability to PDGF-BB.

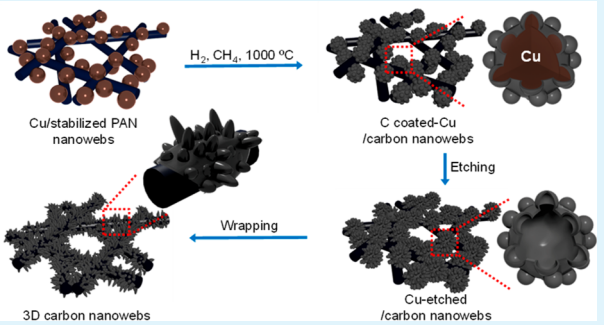

KEYWORDS: *biosensor, oncogenic protein, platelet-derived growth factor, graphene, nanoweb*

INTRODUCTION

Flexible electronics, such as smart cloth, electronic paper, foldable displays, and bendable energy devices, have attracted attention from various fields due to their mechanical properties such as bendability and foldability, which conventional devices do not have.[1−5] Particularly, several studies have been performed on flexible biosensors because such sensors could be used in wearable and implantable point of care monitoring devices.[6−10] However, flexible biosensors have been studied mostly for measuring biophysical parameters (e.g., temperature, heart rate, pH, and intraocular pressure monitoring).[11−15] For this reason, the need to explore the use of flexible biosensors for detecting small biomolecules and biomarkers causing diseases has been felt.[16]

Recently, the sensing of tumor-producing proteins and biomarkers associated with cancer has been focused because of their inherent role in diagnosing diseases.[17−23] In particular, platelet-induced growth factors (PDGFs), which are a dimeric glycoprotein composed of two A components (PDGF-AA), two B components (PDGF-BB), or one of each (PDGF-AB), have emerged as crucial cancer biomarkers of diseases such as atherosclerosis, pulmonary hypertension, organ fibrosis, tumorigenesis, and balloon-injury-induced restenosis.[24−26] Among the divergent PDGFs, PDGF-BB is considered as a latent biomolecule for cancer recognition because it is associated with malignant tumors in humans.[27] To detect PDGF-BB, studies were conducted using different sensing principles such as surface plasmon resonance, fluorescence, and electrochemical redox reactions.[28−32] Among them, the most common method for detecting PDGF-BB is the fluorescence technique, which utilizes changes in fluorescence intensity through energy transfer between fluorophore-labeled aptamer and target analyte. However, this method shows low sensing performance due to conjugation of a fluorophore-labeled aptamer and also presents difficulty in measuring sensing signals in real-time.[33]

Carbon nanomaterials have been studied as key components of transducers in biosensors because of their intrinsic chemical and mechanical properties (such as stability and remarkable electrical conductivity) and large surface areas. Among the various synthesis methods, electrospinning is a popular method to fabricate 1D carbon nanostructures (e.g., carbon nanofibers and carbon nanotubes) because it can easily produce large 1D structures and allows easy post-treatment.[34−37] Despite being a small-sized material, the electrospun 1D carbon nanostructures are agglomerated in a web form and have the limitation of low mechanical properties because of the mesoporous structure generated during the carbonization process.[38−40] These

Received: February 26, 2020
Accepted: April 21, 2020
Published: April 21, 2020

https://dx.doi.org/10.1021/acsami.0c03709
ACS Appl. Mater. Interfaces 2020, 12, 20882−20890

Scheme 1. Schematic Illustration of Fabrication Steps for 3D Carbon Nanoweb-Based Liquid-Ion Gated FET-Type Aptamer Sensor

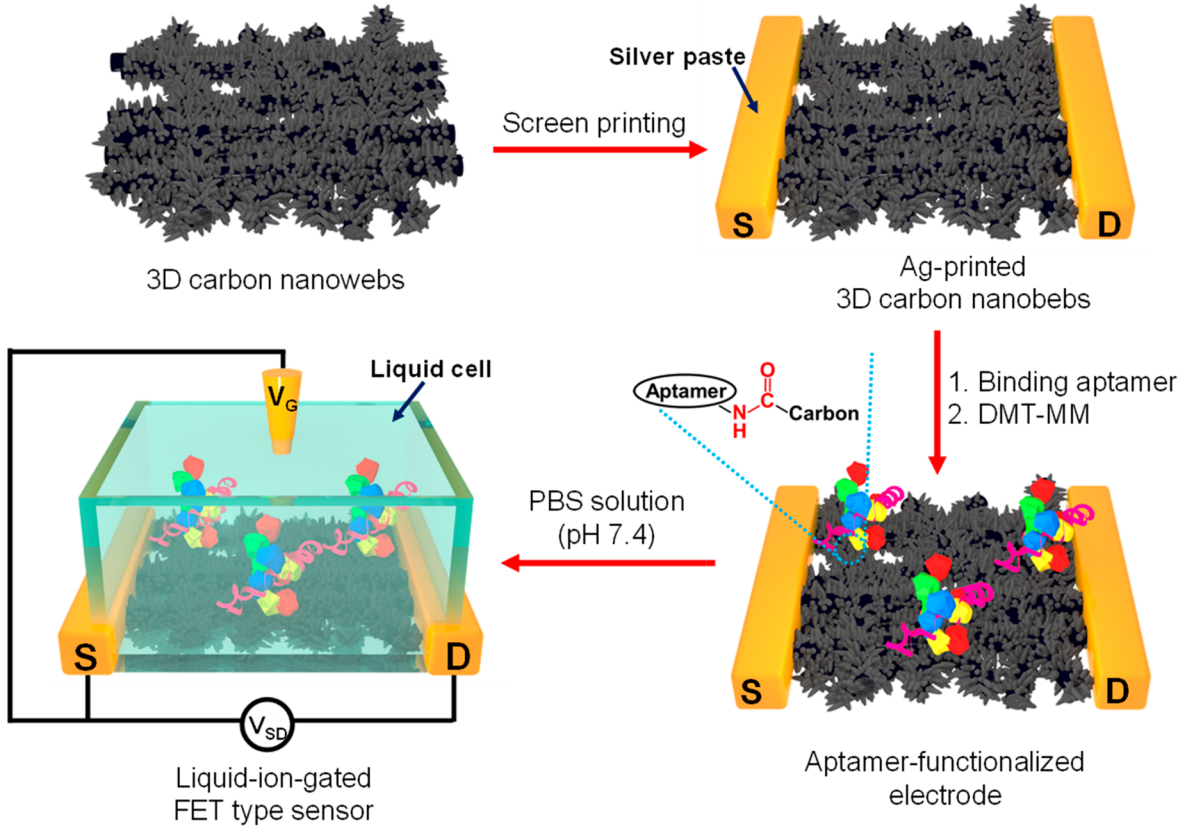

limitations hinder their use in flexible applications and make their post treatment to produce carbon composite nanomaterials difficult.

To increase the interaction between the sensor transducer and analytes, some research groups have focused on expanding the surface area of the transducer using three-dimensional carbon structures.[41−44] First, the 3D N-doped carbon-nanotube-decorated-carbon form hybrids were synthesized using chemical vapor deposition of the melamine resin foam and used for the highly sensitive glucose biosensor.[42] Next, the Ni-nanoparticle-decorated three-dimensional porous carbon was fabricated through chemical reaction of pomelo peels and followed by heat treatment to apply it in the glucose biosensor.[43] However, the fabrication of 3D carbon-based nanocomposites requires a complex experimental process. In addition, the synthesized 3D carbon structures generated by conventional methods have low mechanical strength, making it difficult to use them as flexible devices.

Herein, we report the fabrication of a three-dimensional carbon nanoweb (3DCNW)-based biosensor using electrospinning and chemical vapor deposition (CVD) processes. As a template for the 3D nanostructure, polyacrylonitrile (PAN) nanowebs were synthesized through electrospun and compression processes. Protrusions of carbon were grown on the nanoweb surface through CVD with copper (Cu) powder and Cu etching. Next, PDGF-B binding aptamers were introduced on the 3DCNW surface to form biosensor electrodes. The fabricated free-standing aptamer-functionalized biosensor exhibited a remarkable minimum detectable limit (1.78 fM) of the target analyte (PDGF-BB) with high reversibility, selectivity, and stability. Moreover, its mechanical properties were demonstrated in that its electrical resistance remained unchanged even after being bent repeatedly more than 100 times.

RESULTS AND DISCUSSION

Fabrication of Aptamer-Functionalized 3D Carbon Nanoweb-Based Biosensor. A liquid-ion gated field effect transistor (FET)-type sensor configuration was constructed to study the sensing abilities of the 3DCNW. Scheme 1 illustrates the sequential steps to assemble the sensor. First, a silver paste was printed via screen printing on both ends of the nanoweb. Particularly, 3DCNW was synthesized using facile electrospinning and CVD steps to apply it as a sensing transducer and a template of binding aptamer in the sensing system. Figure 1 shows the sequential steps for fabricating 3DCNWs. As starting materials, polyacrylonitrile nanowebs (PANNWs) were prepared via electrospinning of the PAN solution. The acquired PANNWs were then soaked in deionized water and dried in a physically compressed state to prevent the tangling of nanofibers because of static electricity. The PANNWs were stabilized at 270 °C to convert the branched backbone polymer chain into a ring structure to enhance its crystallinity and mechanical properties. The stabilized PANNWs had a diameter of ca. 600 nm without aggregation (Figure 2a). The stabilized PANNWs were daubed with spherical copper powder (ca. 1 μm in diameter) to form Cu-coated stabilized PANNWs (Figure 2b). Additional bumpy morphology of carbon layers was grown on the Cu surface through a CVD step. During the CVD process, H_2 gas acted as a carrier gas, and CH_4 was the carbon source dissolved in the Cu surface. The CH_4 dissolved in Cu at high temperatures (1000 °C) precipitated to the surface during quenching and formed a

https://dx.doi.org/10.1021/acsami.0c03709
ACS Appl. Mater. Interfaces 2020, 12, 20882−20890

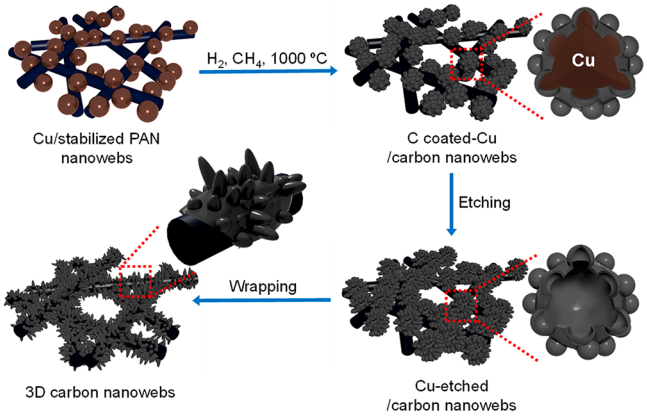

Figure 1. Schematic illustration of the sequential steps for fabricating three-dimensional carbon nanowebs.

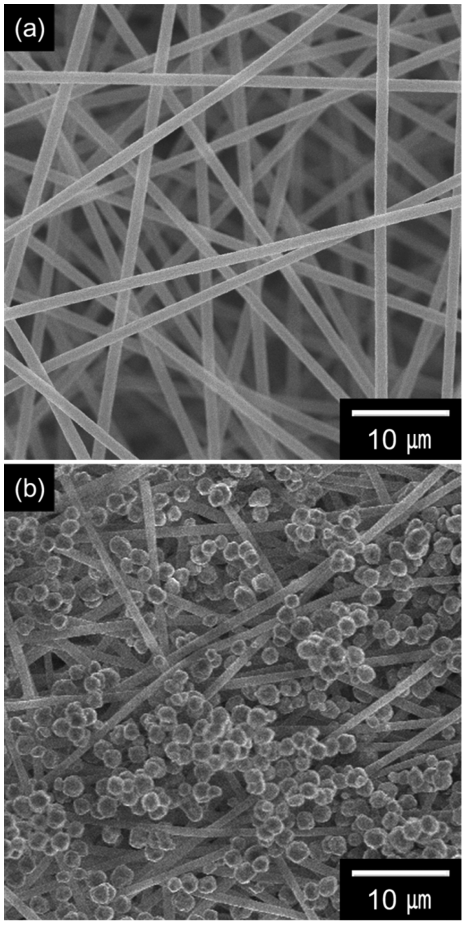

Figure 2. Field-emission scanning electron microscopy (FE-SEM) images of (a) stabilized PAN nanowebs and (b) Cu powder daubed stabilized PAN nanowebs.

carbon layer. Subsequently, carbon-only materials were obtained by removing Cu with a Cu etchant. Figure 3a and b exhibits 3DCNWs consisting of the distinct ca. 400 nm thickness of carbon nanofibers with sharp protrusions on the surface. The process of generating protrusions was as follows: first, rounded Cu protrusions were formed on Cu spheres in the beginning of the CVD process at a high temperature. Next, the carbon layer was formed on the Cu surface as rounded protrusion morphology during the quenching process. The Cu etching

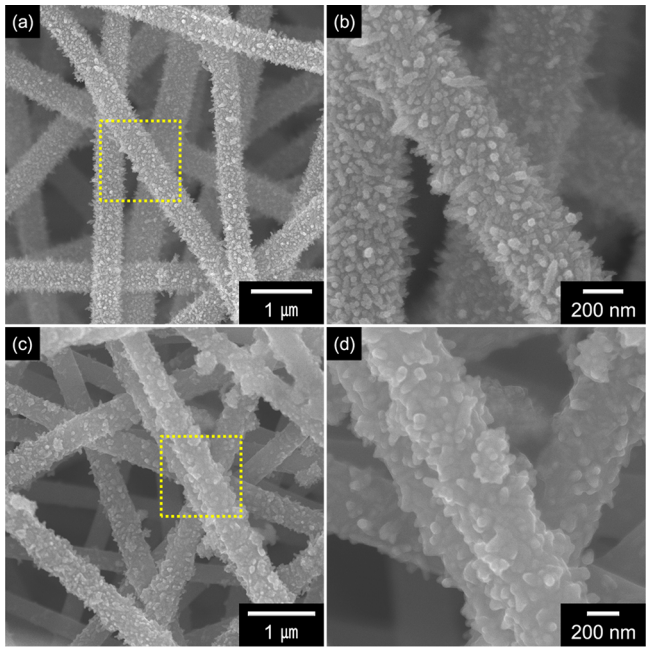

Figure 3. Low- and high-magnification FE-SEM images of (a,b) 3D carbon nanowires and (c,d) PDGF-B binding aptamer immobilized 3D carbon nanowebs.

process was used to hollow the insides of CVD carbon coating layer. Unable to maintain the hollow structure without a Cu template, the morphology of the CVD carbon layer was changed to sharp needles in tandem with wrapping a single carbon nanofiber.[45,46] On the other hand, carbon nanowebs using other copper types (e.g., copper flake (FCNW)) as a template of CVD carbon present the formation of a carbon network in the structure (Figure S1).

X-ray diffraction (XRD) analysis was performed to confirm the removal of Cu after the Cu etching step (Figure S2). Comparing the spectra of 3DCNW with the corresponding Cu sphere spectra, we can be seen that there are no characteristic peaks of Cu. Moreover, the graphite structure of 3DCNW is demonstrated by a strong wide band at 24.6° and a weak band at 43.1°, which correspond to the diffraction of the (002) and (100) planes of sp_2 carbon, respectively.[47,48] Furthermore, the energy-dispersive X-ray spectroscopy element dot mapping analysis of 3DCNW was used to confirm the removal of Cu (Figure S3). Element mapping clearly confirmed the presence of C, N, and O atoms in the 3DCNW. The uniformly distributed C mapping shows that C is well formed, and the structure does not collapse. In addition to the presence of a significant amount of O atoms, it can be seen that there is a functional group containing O atoms such as the hydroxyl and carboxyl groups on the surface. Although the Cu atom mapping and element composition indicate the presence of Cu, its amount is negligible, which means that the Cu removal via etching was successful (Figure S4). Fourier-transform infrared (FT-IR) spectroscopy also confirmed the presence of the carboxyl group (i.e., C═O stretching peak near 1793 cm^{-1}) on the surface (Figure S5). The Cu etchant is an acid solution that enables the simultaneous copper removal and acid treatment of carbon. In this way, the carboxyl group on the carbon surface was generated after the Cu etching step.

To obtain a deeper insight into the properties of the generated carbon layer, Raman spectroscopy was performed. Figure S6

https://dx.doi.org/10.1021/acsami.0c03709
ACS Appl. Mater. Interfaces 2020, 12, 20882−20890

shows the Raman spectra of conventional electrospun carbon nanofibers and 3DCNWs. Both exhibit D (1338.9 cm^{-1}) and G (1581.3 cm^{-1}) bands, which are characteristic bands of carbon materials. For 3DCNWs, the 2D band (2657 cm^{-1}) existed due to the E_{2g} symmetry mode and second-order two-phonon vibration of sp_2 hexagonal with a diminished I_D/I_G ratio (0.935 for 3DCNW) as compared to that of electrospun carbon nanofibers (1.147). On the basis of the 2D peak and decreased I_D/I_G ratio, the protrusion carbon layer has a graphene rather than the conventional sp_2 carbon structure.[49−52]

Thereafter, a PDGF-B binding aptamer and 4-(4,6-dimethoxy-1,3,5-triazin-2-yl)-4-methylmorpholinium chloride) (DMT-MM) mixture was drop-cast on the 3DCNW and dried at 25 °C. The DMT-MM is a well-known organic triazine derivative frequently used for amide synthesis as a condensing agent.[53] The PDGF-B binding aptamer is coated on the 3DCNW surface by covalent bonding (−CONH) between the amino group ($-NH_2$) of the aptamer and the carboxyl group (−COOH) in the carbon structure. The aptamer-functionalized 3DCNW is denoted as A_3DCNW. The liquid-ion gated FET-type configuration was completed by adding a 0.1 M PBS solution (pH 7.4) and applying voltage on the prepared A_3DCNW electrode. Figure 3c and d depicts that the decoration of the binding aptamer changes the morphology of nanofibers from sharp protrusions to a blunt surface and enhances their diameter (ca. 420 nm).

Real-Time Response of Biosensor. To evaluate the electrical properties of the A_3DCNW, the electrical contact and resistance were measured by current−voltage ($I-V$) curves (Figure 4a). Although the binding aptamer is immobilized, $I-V$ curves display linearity (i.e., ohmic contact) in a wide range of voltages. This indicates that the PDGF-B binding aptamer was successfully immobilized on 3DCNW by covalent bonding. In addition, the value of dI/dV (i.e., reciprocal of resistance) is maintained after the decoration of the binding aptamer, which confirms that the electrical property of the electrode is preserved without any deterioration in electrical contact. Moreover, resistance change caused by repeated bending was measured to prove the durability and free-standing properties of the A_3DCNW electrode (Figure 4b). Excellent mechanical durability and flexibility were confirmed after 300 bending cycles. The resistance change was insignificant after 70 bending cycles. After 100 bending cycles, however, the resistance increased, up to 125.1 kΩ at 300 bending cycles, which is 7.94% higher than the initial value (115.9 kΩ) (Table S1).

To investigate the charge transport properties of the electrode, a liquid-ion gated FET-type configuration was adopted by applying the PBS solution (pH 7.4) as an electrolytic gate. Figure 4C shows the source drain current (I_{SD})−source drain voltage (V_{SD}) curves on applying a wide range of gate voltages (V_G) (from −100 to −10 mV) at a constant scan rate of 10 mV s^{-1}. At constant V_{SD}, I_{SD} tended to increase negatively as V_G increased negatively. In other words, negative V_G increased the oxidation level of the carbon channel, exhibiting a p-type behavior.

Figure 5a depicts the real-time response of the A_3DCNW-based biosensors as a function of analyte concentrations. The I_{SD} is monitored and normalized at a low operating voltage (V_G = 10 mV, V_{SD} = 0.1 mV), with a sequential injection of analytes (PDGF-AA, PDGF-AB, and PDGF-BB). When the target analyte (PDGF-BB) was injected, I_{SD} rapidly decreased and saturated within seconds. The decrease in I_{SD} in accordance with the formation of a complex is due to the interaction between the

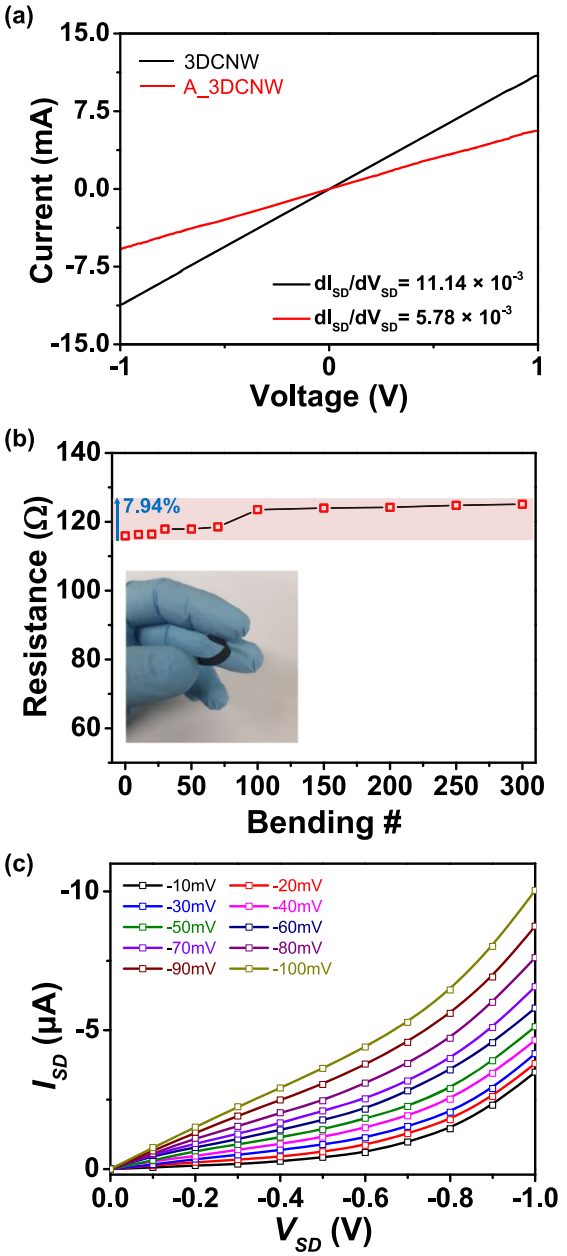

Figure 4. (a) Source-drain current versus source-drain voltage ($I_{SD}-V_{SD}$) for 3DCNW (black) and A_3DCNW (red) electrodes. (b) Resistance changes of A_3DCNW electrode with repetitive bending. (c) $I_{SD}-V_{SD}$ characteristics of A_3DCNW-based liquid-ion gated FET sensors as a function of gate voltage (V_G) from −0.1 to −0.01 V (scan rate of V_{SD}: 10 mV s^{-1}).

PDGF-B binding aptamer and target analyte. To elaborate, the binding aptamer generally shows an overall negative charge in the PBS solution due to the phosphate group in the nucleic acid backbone. When the target analyte reacts with the aptamer, a change in the morphology of the aptamer is induced from a linear form to a complicated tertiary structure. The negative charge on the aptamer strand is weakened by chain folding, thereby decreasing the hole concentration on the surface of the sensor electrode and leading to a decline in the normalized current. This reaction occurs in PDGF-B-containing cases (PDGF-AB and PDGF-BB), whereas PDGF-BB is more sensitive because it can occur in bimolecular directions. Therefore, PDGF-BB shows a lower minimum detectable level

https://dx.doi.org/10.1021/acsami.0c03709
ACS Appl. Mater. Interfaces 2020, 12, 20882−20890

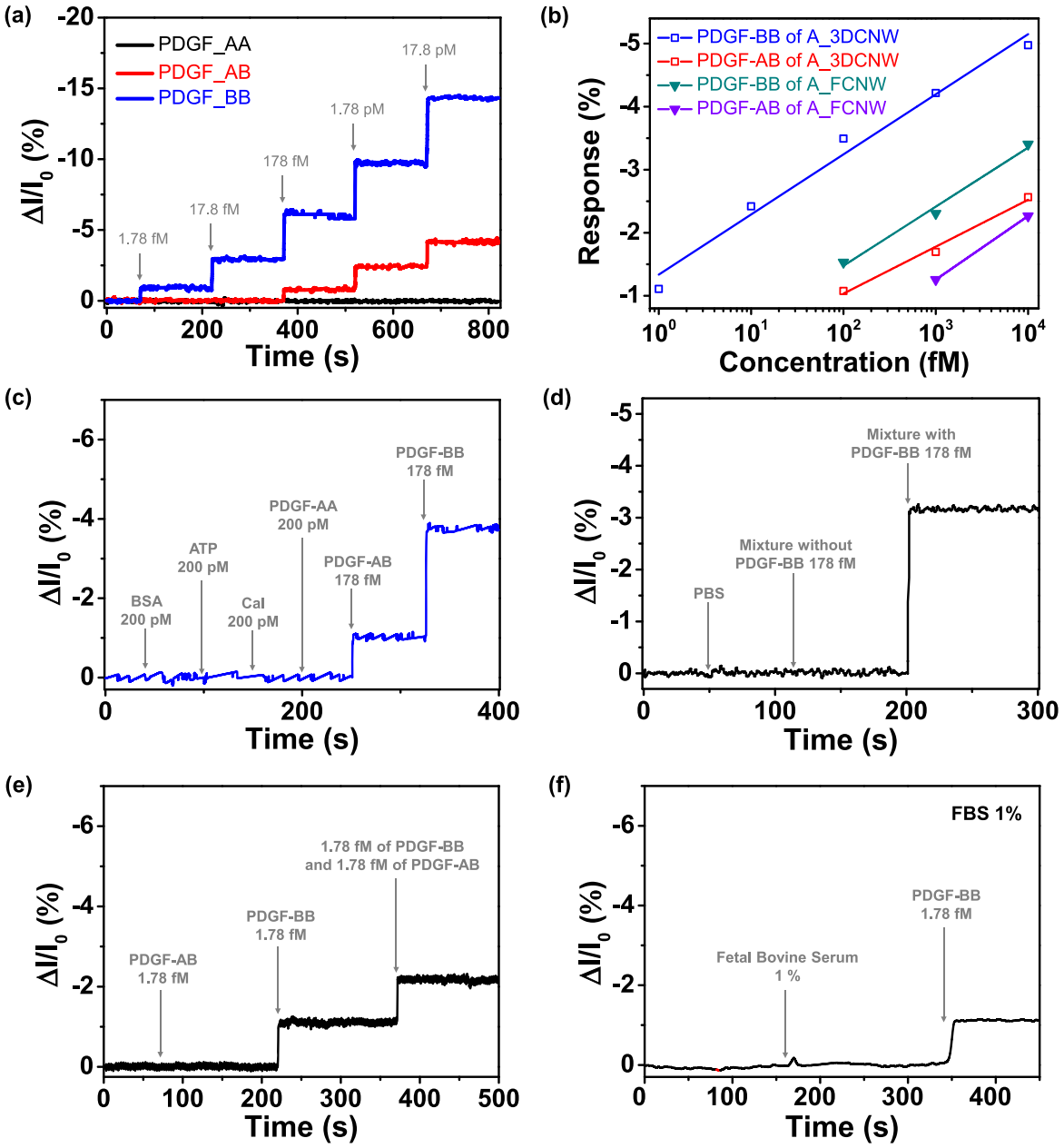

Figure 5. (a) Real-time response with normalized current change of the A_3DCNW toward different PDGFs (black, PDGF-AA; red, PDGF-AB; and blue, PDGF-BB) (V_G = 10 mV and V_{SD} = 0.1 mV). (b) Calibration curves of aptamer-functionalized carbon nanowires with variation of target analytes. (c) Selective response of A_3DCNW toward target (PDGF-AB and PDGF-BB) and nontarget (BSA, ATP, cal., and PDGF-AA) molecules. (d) Selective response of nontarget mixture without PDGF-BB and with PDGF-BB. Real-time response current changes (e) with coexistence of PDGF-AB and PDGF-BB and (f) in diluted fetal bovine serum solution.

(MDL) (1.78 fM) than that of PDGF-AB (178 fM) at the same sensor electrode. In addition, the morphology of carbon nanowebs also affects the value of MDL. The aptamer-functionalized carbon nanowebs from the Cu flake (A_FCNW)-based sensor show a relatively high MDL (1.78 pM) of PEGF-BB (Figure S7). This is because the protrusions on the surface of 3DCNW provide an increased anchoring area for the aptamer corresponding to the high surface area.

Figure 5b presents the response calibration curve as a function of the analyte concentration. The response is defined as the change in the normalized current from before the target analyte injection to the saturated value. Distinctively, biosensors display a linear behavior with respect to a wide range of analyte concentrations. The formulas for obtaining these curves are as follows:

$$S_{\text{PDGF-AB}} \text{ of A\_3DCNW (\%)} = -0.323 \log C + 0.4539$$

$$S_{\text{PDGF-BB}} \text{ of A\_3DCNW (\%)} = -0.414 \log C - 1.3368$$

$$S_{\text{PDGF-AB}} \text{ of A\_FCNW (\%)} = -0.414 \log C + 17708$$

$$S_{\text{PDGF-BB}} \text{ of A\_FCNW (\%)} = -0.407 \log C + 0.3965$$

where C is the concentration of the analyte (PDGF-AB or PDGF-BB) in femtomolar. Therefore, A_3DCNW-based

https://dx.doi.org/10.1021/acsami.0c03709
ACS Appl. Mater. Interfaces 2020, 12, 20882−20890

Table 1. Comparison of Representative Sensors for Detection of PDGF-BB

sensing material	sensor type	linear range	limit of detection	ref
AuNPs[a]/aptamer	SPR[b]	1−1000 pM	0.35 pM	28
magnetic beads/aptamer/dsDNA[c]	fluorescence	0.2−100 nM	0.13 nM	29
AuNPs/aptamer	fluorescence/colorimetry		1 nM	30
diamond/aptamer	fluorescence	4 pM to 100 nM	4 pM	31
Au plate/aptamer	electrochemical	50 pM to 60 nM	50 pM	32
3DCNW/aptamer	FET	1.78 fM to 17.8 pM	1.78 fM	this work

[a]Au nanoparticles. [b]Surface plasmon resonance. [c]Double-stranded DNA.

electrode presents superb sensing performance as compared to that of other aptasensors due to a 3D structure of carbon transducer that increases the anchoring area of the binding aptamer (Table 1).

Selectivity is a significant parameter while evaluating the performance of a sensor device. We used common serum proteins such as calmodulin (cal.), adenosine triphosphate (ATP), and bovine serum albumin (BSA) as nontarget molecules to evaluate the selectivity of the biosensor. As shown in Figure 5c, no significant change in the current was observed when various nontarget analytes (200 pM) were injected. On the contrary, exposure to 178 fM target molecules induced a rapid decrease in the normalized current. Moreover, considering the incorporation of PDGF molecules with various substances in the body, the real-time response toward nontarget mixtures was observed (Figure 5d). No significant change in the current was observed when the nontarget mixture was added; however, the nontarget mixture with 178 fM of PDGF-BB exhibited a rapid decrease in the current. It was also confirmed that the PBS solution only contributed to the formation of the dielectric layer in the absence of a significant current change even when injecting a 0.1 M PBS solution. To further check the interference of PDGF-AB with PDGF-BB detection, two molecules at a low detection level (1.78 fM) were tested. As shown in Figure 5e, PDGF-BB shows a significant current change regardless of whether PDGF-AB exists or not. In addition, we conducted the PDGF-BB selectivity test in real biological solution using fetal bovine serum (FBS). Although the detection of the PDGF-BB in FBS was slower than in other cases, a change in current is clearly identified (Figure 5f).

To be applied in real life of the sensor electrode, it is necessary to show certain signal changes even in repeated performance measurements. First, the change in current signal due to repetition of the same concentration (1.78 fM) shows that the signal for repeated measurements tends to decrease in small quantities, but differs by less than 10% from the new electrode (Figure 6a). The stability of the biosensor with 178 fM of PDGF-BB molecules is also depicted in Figure 6b. The sensor electrode was stored at 25 °C in a plastic vessel without any sealing during the stability test. Under this condition, the amount of response decreased by 12.14% for 2 weeks. This relevant decrease is attributed to the inactivation of the PDGF-BB aptamer and destruction of the 3D carbon structure during repetitive measurements.

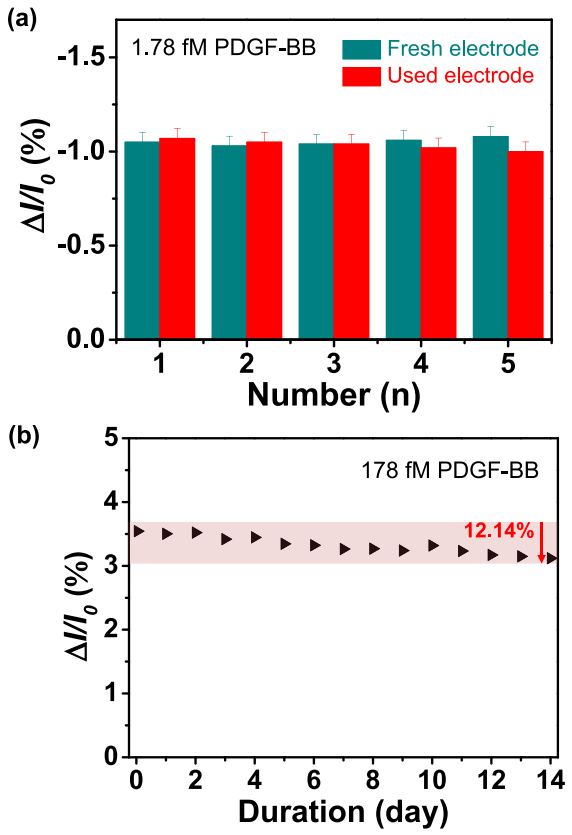

Figure 6. (a) Repeat ability (for 1.78 fM of PDGF-BB) and (b) long-term stability (for 178 fM of PDGF-BB) of A_3DCNW aptasensor.

CONCLUSION

In summary, a free-standing 3DCNW-based biosensor was fabricated using electrospinning, CVD, and immobilization of a binding aptamer in the carbon structure. The sharp carbon protrusions originating from the CVD process generated a 3D structure of carbon nanowebs, which enhance the decoration amount of binding aptamers, thereby improving its attraction for the target analyte (PDGF-BB). The A_3DCNW sensor showed real-time responses with ultrahigh sensitivity to PDGF-BB (1.78 fM), significantly higher than other biosensors. Furthermore, the biosensor showed selectivity to PDGF-BB in nontarget mixed solutions and exhibited long-term stability (2 weeks in this study) with repetitive detections due to covalent bonding between the binding aptamer and carbon surface. To the best of our knowledge, this study is the first demonstration of the 3D graphene layer decoration on the 1D carbon structure to be used in a biosensor transducer. It can have applications as electrode materials in various types of sensor devices, flexible and free-standing, for biological and environmental research.

EXPERIMENTAL SECTION

Materials. PAN (M_w = 150 000), copper etchant, PDGF-AA, PDGF-AB, PDGF-BB, calmodulin (cal.), ATP, and BSA were purchased from Aldrich Chemical Co. The PDGF-B binding aptamer was purchased from Bioneer Co. (Dajeon, Korea) and modified at the 5-terminus with an amine group (5′-NH_2 CAG GCT ACG GCA CGT AGA GCA TCA CCA TGA TCC TG-3′). *N*,*N*-Dimethylformamide

https://dx.doi.org/10.1021/acsami.0c03709
ACS Appl. Mater. Interfaces 2020, 12, 20882−20890

(DMF) was purchased from Junsei Chemical Co., Ltd. Spherical and flaky Cu powders were purchased from Join M (Nonsan, Korea).

Fabrication of Stabilized PANNWs. PAN (13 wt %) was dissolved in DMF at 70 °C for 4 h. The PAN solution was electrospun through a stainless steel needle connected to a high-voltage power supply (10 kV) at 5 μL/min feeding rate. Next, the electrospun PANNWs were soaked in deionized water and dried in a physically compressed state. The compressed PANNWs were heated to 270 °C at a constant heating rate of 1 °C min^{-1} and stabilized for 1 h in ambient air.

Fabrication of 3DCNWs. Different types of Cu powders, flake (average size of 2−3 μm) and sphere (average diameter of 1 μm), were coated on the stabilized PANNWs. The Cu-coated PANNWs were placed in a chamber and heated to 1000 °C at 147 mTorr (H_2) at a flow rate of 8 sccm. This condition was maintained for 30 min to eliminate the copper oxide layer and stabilize the chamber atmosphere. Next, methane (CH_4) gas was fed to the chamber at a flow rate of 20 sccm for 30 min. Thereafter, the furnace chamber was cooled to 25 °C at a rate of 40 °C min^{-1}. Finally, 3DCNWs were fabricated by etching with the Cu powder and rinsing with deionized water several times.

Fabrication of 3DCNW-Based Biosensor. A silver paste was pasted on both ends of the 3DCNW to construct FET sensor configuration. The PDGF-B binding aptamer and DMT-MM mixture were drop-cast on the 3DCNW and dried at 25 °C for 12 h. Afterward, the A_3DCNW electrode was rinsed with distilled water and dried at 25 °C. Next, a 0.1 M PBS solution (pH 7.4) was filled in a solution chamber (volume: 200 μL).

Electrical Measurement of 3DCNW-Based Biosensor. All electrical measurements were performed with a Keithley 2612 SourceMeter, Probe Station (MS TECH, model 4000), and an automatic battery cycler (Wonatech WBCS 3000). The change in the current was normalized by the following equation:

$$S = \left[\frac{\Delta I}{I_0}\right]_{SD} (\%) = \frac{(I - I_0)}{I_0}$$

where S is the sensitivity, I is the measured real-time current, and I_0 is the initial resistance.

Characterization. FE-SEM micrographs were obtained with a JEOL 6700 instrument. JEOL JEM-200CX was used to acquire TEM micrographs. XPS and XRD experiments were performed on JPS-9000MS (JEOL; Mg Kα X-ray source) and M18XHF-SRA (Rigaku SmartLab; λ = 1.5418 Å) instruments, respectively. Raman spectra were acquired on an FRA 1106/S FT-Raman (Bruker) spectrometer and excited with a 514 nm Ar laser. The two-probe method was used to measure the resistance changes according to the number of bending tests.

■ ASSOCIATED CONTENT

Supporting Information

The Supporting Information is available free of charge at https://pubs.acs.org/doi/10.1021/acsami.0c03709.

(1) Morphology of FCNW, (2) XRD spectra of 3DCNW, (3) elemental mapping of 3DCNW, (4) chemical composition of 3DCNW, (5) FT-IR spectra of 3DCNW, (6) Raman spectra of 3DCNW, (7) electrical resistance of A_3DCNW, and (8) sensing performance of Cu flake-derived carbon-based FET sensor (PDF)

■ AUTHOR INFORMATION

Corresponding Authors

Jyongsik Jang − *School of Chemical and Biological Engineering, Seoul National University, Seoul 151-742, Republic of Korea;* orcid.org/0000-0002-0415-802X; Phone: +82-2-880-7069; Email: jsjang@plaza.snu.ac.kr; Fax: +82-2-880-1604

Jun Seop Lee − *Department of Materials Science and Engineering, Gachon University, Seongnam-Si, Gyeonggi-Do 13120, Republic of Korea;* orcid.org/0000-0002-7350-2875; Phone: +82-31-750-5814; Email: junseop@gachon.ac.kr; Fax: +82-31-750-5389

Author

Wooyoung Kim − *School of Chemical and Biological Engineering, Seoul National University, Seoul 151-742, Republic of Korea*

Complete contact information is available at: https://pubs.acs.org/10.1021/acsami.0c03709

Notes

The authors declare no competing financial interest.

■ ACKNOWLEDGMENTS

This work was supported by Device Business, Samsung Electronics, Korea.

■ REFERENCES

(1) Zhao, X.; Zhang, X.; Xue, Z.; Chen, W.; Zhou, Z.; Mu, T. Fe Nanodot-Decorated MoS_2 Nanosheets on Carbon Cloth: an Efficient and Flexible Electrode for Ambient Ammonia Synthesis. *J. Mater. Chem. A* **2019**, *7*, 27417−27422.

(2) Jin, L.; Zheng, Y.; Liu, Z.; Li, J.; Zhai, H.; Chen, Z.; Li, Y. Design of an Ultrasensitive Flexible Bend Sensor Using a Silver-Doped Oriented Poly(vinylidene fluoride) Nanofiber Web for Respiratory Monitoring. *ACS Appl. Mater. Interfaces* **2020**, *12*, 1359−1367.

(3) Man, P.; He, B.; Zhang, Q.; Zhou, Z.; Li, C.; Li, Q.; Wei, L.; Yao, Y. A One-Dimensional Channel Self-Standing MOF Cathode for Ultrahigh-Energy-Density Flexible Ni−Zn Batteries. *J. Mater. Chem. A* **2019**, *7*, 27217−27224.

(4) Zhang, T.; Yang, P.; Chen, M.; Yang, K.; Cao, Y.; Li, X.; Tang, M.; Chen, W.; Zhou, X. Constructing a Novel Electroluminescent Device with High-Temperature and High-Humidity Resistance based on a Flexible Transparent Wood Film. *ACS Appl. Mater. Interfaces* **2019**, *11*, 36010−36019.

(5) Wang, J.; Jiao, J.; Sun, G.; Yuan, K.; Guan, Z.; Wei, X. Preparation and Microwave Absorption Performance of a Flexible Fe_3O_4/Nanocarbon Hybrid Buckypaper and Its Application in Composite Materials. *RSC Adv.* **2019**, *9*, 37870−37881.

(6) Solis-Tinoco, V.; Marqueza, S.; Quesada-Lopez, T.; Villarroy, F.; Homs-Corbera, A.; Lechuga, L. M. Building of a Flexible Microfluidic Plasmo-Nanomechanical Biosensor for Live Cell Analysis. *Sens. Actuators, B* **2019**, *291*, 48−57.

(7) Shin, M.; Yoon, J.; Yi, C.; Lee, T.; Choi, J.-W. Flexible HIV-1 Biosensor Based on the Au/MoS_2 Nanoparticles/Au Nanolayer on the PET Substrate. *Nanomaterials* **2019**, *9*, 1076.

(8) Rosati, G.; Ravarotto, M.; Scaramuzza, M.; Toni, A. D.; Paccagnell, A. Silver Nanoparticles Inkjet-Printed Flexible Biosensor for Rapid Label-Free Antibiotic Detection in Milk. *Sens. Actuators, B* **2019**, *280*, 280−289.

(9) Hou, L.; Zhao, H.; Bi, S.; Zhu, L.; Xu, Y.; Lu, Y. Ultrasensitive and Highly Flexible Nonenzymatic Glucose Biosensor Based on Laser-Scribed Carbon Paper Substrate. *Appl. Surf. Sci.* **2019**, *465*, 320−331.

(10) Kim, Y.-J.; Saviers, K. R.; Fisher, T. S.; Irazoqui, P. P. Continuous Glucose Monitoring with a Flexible Biosensor and Wireless Data Acquisition System. *Sens. Actuators, B* **2018**, *275*, 237−243.

(11) Cheng, Y.; Wu, D.; Hao, S.; Jie, Y.; Cao, X.; Wang, N.; Wang, Z. L. Highly Stretchable Triboelectric Tactile Sensor for Electronic Skin. *Nano Energy* **2019**, *64*, 103907.

(12) Kim, K. K.; Ha, I.; Won, P.; Seo, D. G.; Cho, K. J.; Ko, S. H. Transparent Wearable Three-Dimensional Touch by Self-Generated Multiscale Structure. *Nat. Commun.* **2019**, *10*, 2582.

(13) Patil, A. B.; Huang, Y.; Ma, L.; Wu, R.; Meng, Z.; Kong, L.; Zhang, Y.; Zhang, W.; Liu, Q.; Liu, X. Y. An Efficient Disposable and Flexible Electrochemical Sensor Based on a Novel and Stable Metal Carbon Composite Derived from Cocoon Silk. *Biosens. Bioelectron.* **2019**, *142*, 111595.

(14) Rajendran, V.; Mohan, A. M. V.; Jayaraman, M.; Nakagawa, T. All-Printed, Interdigitated, Freestanding Serpentine Interconnects Based Flexible Solid State Supercapacitor for Self Powered Wearable Electronics. *Nano Energy* **2019**, *65*, 104055.
(15) Yuan, H.; Lei, T.; Qin, Y.; Yang, R. Flexible Electronic Skins Based on Piezoelectric Nanogenerators and Piezotronics. *Nano Energy* **2019**, *59*, 84−90.
(16) Xu, M.; Yadavalli, V. K. Flexible Biosensors for the Impedimetric Detection of Protein Targets Using Silk-Conductive Polymer Biocomposites. *ACS Sens.* **2019**, *4*, 1040−1047.
(17) Deepa, A.; Pundir, S.; Pundir, C. S. Detection of Tumor Suppressor Protein p53 with Special Emphasis on Biosensors: A Review. *Anal. Biochem.* **2020**, *588*, 113473.
(18) Kwon, Y. V.; Zhao, B.; Xu, C.; Lee, J.; Chen, C.-L.; Vinayagam, A.; Edgar, B. A.; Perrimon, N. The Role of Translationally Controlled Tumor Protein in Proliferation of Drosophila Intestinal Stem Cells. *Proc. Natl. Acad. Sci. U. S. A.* **2019**, *116*, 26591−26598.
(19) Pan, J.; Peng, R.; Cheng, N.; Chen, F.; Gao, B. LNK Protein: Low Expression in Human Colorectal Carcinoma and Relationship with Tumor Invasion. *Biomed. Pharmacother.* **2020**, *121*, 109467.
(20) Weng, W.; Zhang, P.; Ruan, J.; Zhang, Y.; Ba, D.; Tang, Y. Prognostic Significance of the Tumor Suppressor Protein p53 Gene in Childhood Acute Lymphoblastic Leukemia. *Oncol. Lett.* **2019**, *19*, 549−556.
(21) Agnes, M.; Nitti, A.; Vander Griend, D. A.; Dondi, D.; Merli, D.; Pasini, D. A Chiroptical Molecular Sensor for Ferrocene. *Chem. Commun.* **2016**, *52*, 11492−11495.
(22) Hao, C.; Xu, L.; Kuang, H.; Xu, C. Artificial Chiral Probes and Bioapplications. *Adv. Mater.* **2019**, 1802075.
(23) Nitti, A.; Pasini, D. Aggregation-Induced Circularly Polarized Luminescence: Chiral Organic Materials for Emerging Optical Technologies. *Adv. Mater.* **2020**, 1908021.
(24) Barst, R. J. PDGF Signaling in Pulmonary Arterial Hypertension. *J. Clin. Invest.* **2005**, *115*, 2691−2694.
(25) Hosaka, K.; Yang, Y.; Seki, T.; Nakamura, M.; Andersson, P.; Rouhi, P.; Yang, X.; Jensen, L.; Lim, S.; Feng, N.; Xue, Y.; Li, X.; Larsson, O.; Ohhashi, T.; Cao, Y. Tumour PDGF-BB Expression Levels Determine Dual Effects of Anti-PDGF Drugs on Vascular Remodeling and Metastasis. *Nat. Commun.* **2013**, *4*, 2129.
(26) Lin, T. E.; Chen, W. H.; Shiang, Y. C.; Huang, C. C.; Chang, H. T. Colorimetric Detection of Platelet-Derived Growth Factors Through Competitive Interactions Between Proteins and Functional Gold Nanoparticles. *Biosens. Bioelectron.* **2011**, *29*, 204−209.
(27) Li, F.; Yu, F.; Liao, X.; Wu, C.; Wang, Y.; Li, C.; Lou, F.; Li, B.; Yin, B.; Wang, C.; Ye, L. Efficacy of Recombinant Human BMP2 and PDGF-BB in Orofacial Bone Regeneration: A Systematic Review and Meta-analysis. *Sci. Rep.* **2019**, *9*, 8073.
(28) Qian, H.; Huang, Y.; Duan, X.; Wei, X.; Fan, Y.; Gan, D.; Yue, S.; Cheng, W.; Chen, T. Fiber Optic Surface Plasmon Resonance Biosensor for Detection of PDGF-BB in Serum Based on Self-Assembled Aptamer and Antifouling Peptide Monolayer. *Biosens. Bioelectron.* **2019**, *140*, 111350.
(29) Bahreyni, A.; Tahmasebi, S.; Ramezani, M.; Alibolandi, M.; Danesh, N. M.; Abnous, K.; Taghdisi, S. M. A Novel Fluorescent Aptasensor for Sensitive Detection of PDGF-BB Protein Based on a Split Complementary Strand of Aptamer and Magnetic Beads. *Sens. Actuators, B* **2019**, *280*, 10−15.
(30) Shukoor, M. I.; Altman, M. O.; Han, D.; Bayrac, A. T.; Ocsoy, I.; Zhu, Z.; Tan, W. Aptamer-Nanoparticle Assembly for Logic-Based Detection. *ACS Appl. Mater. Interfaces* **2012**, *4*, 3007−3011.
(31) Ruslinda, A. R.; Penmatsa, V.; Ishii, Y.; Tajima, S.; Kawarada, H. Highly Sensitive Detection of Platelet-Derived Growth Factor on a Functionalized Diamond Surface Using Aptamer Sandwich Design. *Analyst* **2012**, *137*, 1692−1697.
(32) Lai, R. Y.; Plaxco, K. W.; Heeger, A. J. Aptamer-Based Electrochemical Detection of Picomolar Platelet-Derived Growth Factor Directly in Blood Serum. *Anal. Chem.* **2007**, *79*, 229−233.
(33) Yang, C. J.; Jockusch, S.; Vicens, M.; Turro, N. J.; Tan, W. Light-Switching Excimer Probes for Rapid Protein Monitoring in Complex Biological Fluids. *Proc. Natl. Acad. Sci. U. S. A.* **2005**, *102*, 17278−17283.
(34) Kim, G. H.; Nam, H.; Choi, W.; An, T.; Lim, G. Electrospinning Nanofiber on an Insulating Surface with a Patterned Functional Electrolyte Electrode. *Adv. Mater. Interfaces* **2018**, *5*, 1701204.
(35) Lee, J. H.; Kim, J.; Liu, D.; Guo, F.; Shen, X.; Zheng, Q.; Jeon, S.; Kim, J. K. Highly Aligned, Anisotropic Carbon Nanofiber Films for Multidirectional Strain Sensors with Exceptional Selectivity. *Adv. Funct. Mater.* **2019**, *29*, 1901623.
(36) Xue, J.; Wu, T.; Dai, Y.; Xia, Y. Electrospinning and Electrospun Nanofibers: Methods, Materials, and Applications. *Chem. Rev.* **2019**, *119*, 5298−5415.
(37) Yoon, J.; Yang, H. S.; Lee, B. S.; Yu, W. R. Recent Progress in Coaxial Electrospinning: New Parameters, Various Structures, and Wide Applications. *Adv. Mater.* **2018**, *30*, 1704765.
(38) Dai, Z.; Ren, P.-G.; Jin, Y.-L.; Zhang, H.; Ren, F.; Zhang, Q. Nitrogen-Sulphur Co-Doped Graphenes Modified Electrospun Lignin/Polyacrylonitrile-Based Carbon Nanofiber as High Performance Supercapacitor. *J. Power Sources* **2019**, *437*, 226937.
(39) Jia, H.; Sun, N.; Dirican, M.; Li, Y.; Chen, C.; Zhu, P.; Yan, C.; Zang, J.; Guo, J.; Tao, J.; Wang, J.; Tang, F.; Zhang, X. Electrospun Kraft Lignin/Cellulose Acetate-Derived Nanocarbon Network as an Anode for High-Performance Sodium-Ion Batteries. *ACS Appl. Mater. Interfaces* **2018**, *10*, 44368−44375.
(40) Jagadale, A.; Zhou, X.; Blaisdell, D.; Yang, S. Carbon Nanofibers (CNFs) Supported Cobalt-Nickel Sulfide ($CoNi_2S_4$) Nanoparticles Hybrid Anode for High Performance Lithium Ion Capacitor. *Sci. Rep.* **2018**, *8*, 1602.
(41) Mendes, R. G.; Wróbel, P. S.; Bachmatiuk, A.; Sun, J.; Gemming, T.; Liu, Z.; Rümmeli, M. H. Carbon Nanostructures as a Multi-Functional Platform for Sensing Applications. *Chemosensors* **2018**, *6*, 60.
(42) Ma, Y.; Song, X.; Ge, X.; Zhang, H.; Wang, G.; Zhang, Y.; Zhao, H. In Situ Growth of α-Fe_2O_3 Nanorod Arrays on 3D Carbon Foam as an Efficient Binder-Free Electrode for Highly Sensitive and Specific Determination of Nitrite. *J. Mater. Chem. A* **2017**, *5*, 4726−4736.
(43) Fan, P.; Liu, L.; Guo, Q.; Wang, J.; Yang, J.; Guan, X.; Chen, S.; Hou, H. Three-Dimensional N-doped Carbon Nanotube@Carbon Foam Hybrid: an Effective Carrier of Enzymes for Glucose Biosensors. *RSC Adv.* **2017**, *7*, 26574−26582.
(44) Wang, L.; Zhang, Y.; Yu, J.; He, J.; Yang, H.; Ye, Y.; Song, Y. A Green and Simple Strategy to Prepare Graphene Foam-Like Three-Dimensional Porous Carbon/Ni Nanoparticles for Glucose Sensing. *Sens. Actuators, B* **2017**, *239*, 172−179.
(45) Yang, J.; Qian, X.; Li, H.; Wang, H.; Xue, X.; Cai, L.; Hu, P.; Yu, G. Novel Hollow Graphene Flowers Synthesized by Cu-Assisted Chemical Vapor Deposition. *Adv. Mater. Interfaces* **2018**, *5*, 1800347.
(46) Wang, H.; Gao, E.; Liu, P.; Zhou, D.; Geng, D.; Xue, X.; Wang, L.; Jiang, K.; Xu, Z.; Yu, G. Facile Growth of Vertically-Aligned Graphene Nanosheets via Thermal CVD: The Experimental and Theoretical Investigations. *Carbon* **2017**, *121*, 1−9.
(47) Mardiansyah, D.; Badloe, T.; Triyana, K.; Mehmood, M. Q.; Raeis-Hosseini, N.; Lee, Y.; Sabarman, H.; Kim, K.; Rho, J. Effect of Temperature on the Oxidation of Cu Nanowires and Development of an Easy to Produce, Oxidation-Resistant Transparent Conducting Electrode Using a PEDOT:PSS Coating. *Sci. Rep.* **2018**, *8*, 10639.
(48) Elzey, S.; Baltrusaitis, J.; Bian, S.; Grassian, V. H. Formation of Paratacamite Nanomaterials via the Conversion of Aged and Oxidized Copper Nanoparticles in Hydrochloric Acidic Media. *J. Mater. Chem.* **2011**, *21*, 3162−3169.
(49) Lin, Y.; Watson, K. A.; Fallbach, M. J.; Ghose, S.; Smith, J. G., Jr.; Delozier, D. M.; Cao, W.; Crooks, R. E.; Connell, J. W. Rapid, Solventless, Bulk Preparation of Metal Nanoparticle-Decorated Carbon Nanotubes. *ACS Nano* **2009**, *3*, 871−884.
(50) Cao, Y.; Lu, H.; Hong, Q.; Xu, B.; Wang, J.; Deng, Y.; Yang, W.; Cai, W. Synthesis of Ag/Co@CoO NPs Anchored Within N-Doped Hierarchical Porous Hollow Carbon Nanofibers as a Superior Free-Standing Cathode for Li-O_2 Batteries. *Carbon* **2019**, *144*, 280−288.

https://dx.doi.org/10.1021/acsami.0c03709
ACS Appl. Mater. Interfaces 2020, 12, 20882−20890

(51) Park, K. D.; Raschke, M. B.; Atkin, J. M.; Lee, Y. H.; Jeong, M. S. Probing Bilayer Grain Boundaries in Large-Area Graphene with Tip-Enhanced Raman Spectroscopy. *Adv. Mater.* **2017**, *29*, 1603601.
(52) Chen, X.; Xiang, R.; Zhao, P.; An, H.; Inoue, T.; Chiashi, S.; Maruyama, S. Chemical Vapor Deposition Growth of Large Single-Crystal Bernal-Stacked Bilayer Graphene from Ethanol. *Carbon* **2016**, *107*, 852−856.
(53) Wang, R.; Lu, D.; Bai, H.; Jin, C.; Yan, G.; Ye, M.; Qiu, L.; Chang, R.; Cui, C.; Liang, H.; Tan, W. Using Modified Aptamers for Site Specific Protein−Aptamer Conjugations. *Chem. Sci.* **2016**, *7*, 2157−2161.

https://dx.doi.org/10.1021/acsami.0c03709
ACS Appl. Mater. Interfaces 2020, 12, 20882−20890